Exploring interacting chiral spin chains in terms of black hole physics

Ewan Forbes [1], Matthew D. Horner [1,2], Andrew Hallam [1], Joseph Barker [1], and Jiannis K. Pachos [1]

[1]*School of Physics and Astronomy, University of Leeds, Leeds LS2 9JT, United Kingdom*
[2]*Aegiq Ltd., Cooper Buildings, Sheffield S1 2NS, United Kingdom*

In this paper we explore the properties of a one-dimensional spin chain in the presence of chiral interactions, focusing on the system's transition to distinct chiral phases for various values of the chiral coupling. By employing the mean-field theory approximation we establish a connection between this chiral system and a Dirac particle in the curved spacetime of a black hole. Surprisingly, the black-hole horizon coincides with the interface between distinct chiral phases. We examine the chiral properties of the system for homogeneous couplings and in scenarios involving position-dependent couplings that correspond to black-hole geometries. To determine the significance of interactions in the chiral chain we employ bosonization techniques and derive the corresponding Luttinger liquid model. Furthermore, we investigate the classical version of the model to understand the impact of the chiral operator on the spins and gain insight into the observed chirality. Our findings shed light on the behavior of the spin chain under the influence of the chiral operator, elucidating the implications of chirality in various contexts, including black-hole physics.

I. INTRODUCTION

An intriguing family of lattice models can be described by relativistic physics in their continuum limit. One prominent illustration of this phenomenon is graphene, whose behavior at low energy can be effectively described by the renowned Dirac equation [1,2]. Similar relativistic descriptions can be found in diverse examples such as Kitaev's honeycomb model [3,4], superconductors [5,6], and the XX model [7,8]. These relativistic frameworks not only deepen our understanding of these systems but also pave the way for the simulation of high-energy physics with table-top experiments.

In this paper, we explore a chiral modification of the one-dimensional (1D) spin-1/2 XX model [9]. The XX model can be expressed in terms of free fermions and thus it is analytically tractable and well understood. The introduction of a three-spin chiral term renders it interacting and thus hard to investigate analytically or numerically. It is noteworthy that such chiral systems exhibit a rich spectrum of quantum correlations [10] and they can give rise to skyrmions [11]. Remarkably, we demonstrate that these chiral systems can be effectively modeled by the Dirac equation on a curved spacetime. This intriguing connection offers a unique opportunity to realize a black-hole background within the laboratory setting.

The emergent black-hole physics is explicitly revealed by applying the mean-field (MF) approximation, and its existence can be verified by investigating the Hawking effect.

Hawking radiation, resulting from vacuum fluctuations of quantum fields near a black hole's horizon, leads to the evaporation of the black-hole [12,13]. The mechanism used to find this [9], involving a wave packet tunneling across the horizon and escaping with a thermal distribution, originally derived in Ref. [14], allows the simulation of Hawking radiation in fermionic lattice models [15–30]. We test the reliability of this approximation through a detailed analysis of the bosonization of the full spin model. We find that the MF approximation faithfully predicts a phase transition between a chiral and nonchiral phase. Remarkably, the emergent event horizon aligns with the interface between chiral and nonchiral phases. In particular, we find that the inside of the black hole corresponds to a chiral region with a central charge of $c = 2$ where the chiral interaction is dominant. The outside corresponds to a nonchiral region where the XX model is dominant, with a central charge $c = 1$. Subsequently, we examine the MF approximation's validity by employing bosonization techniques, of which a general case has been studied for two [31,32] and four [33] Fermi points, which allows us to map the fully interacting Hamiltonian onto a Luttinger liquid [32]. Additionally, we employ a classical version of the system to further analyze and understand these effects in a comprehensive manner. By doing so, we gain valuable insights into the impact of chirality on the spins along the chain and its consequential effects on the entire system. We envision that the presented geometric description provides an elegant formalism to model strongly interacting systems and their interfaces also in higher dimensions and thus predict their behavior.

This article is organized as follows: In Sec. II we introduce our model and then diagonalize it to highlight the characteristics of the system, such as the transition in the dispersion relation due to the effect of the chiral order parameter. In Sec. III we give an effective description of the chiral chain
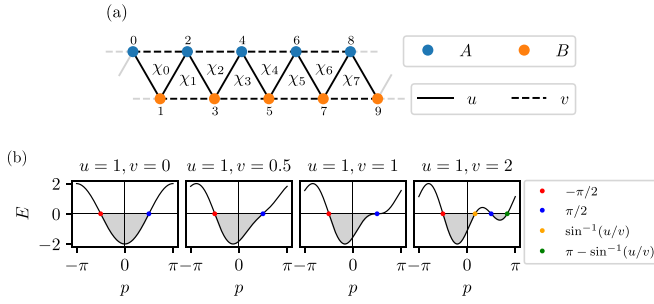
FIG. 1. (a) The interactions of the lattice diagrammatically portrayed with nearest-neighbor interaction strength defined by u and next-to-nearest neighbor interactions by v [9], with the seperations of neighboring spins into groups A and B representing the unit cell described in Eq. (18). The chirality operator calculates the interaction of the three spins in each triangular space [11]. (b) The dispersion relation of the Hamiltonian for various values of v. We see that two additional Fermi points appear if $v > u$ which divides the negative-energy portion of the Brillouin zone into two disconnected regions.

in terms of black-hole geometry. In Sec. IV we investigate the chiral spin operator and its expectation with the ground state of the system both in the flat and curved space cases. In Sec. V we use bosonization to ascertain the significance of the interactions, and in Sec. VI we use a classical version of the system to gain a geometric intuition on chiral interactions. We give concluding remarks and an outlook in Sec. VII.

II. CHIRAL CHAIN MODEL

Here we introduce the chiral spin chain, transform it to interacting fermions, and then apply mean-field theory to determine its properties.

A. The mean-field approximation

The system we investigate here is the one-dimensional spin-$\frac{1}{2}$ chain with the Hamiltonian

$$H = \sum_{n=0}^{N-1} \left[-\frac{u}{2} \left(\sigma_n^x \sigma_{n+1}^x + \sigma_n^y \sigma_{n+1}^y \right) - \frac{v}{4} \chi_n \right], \quad (1)$$

where the spin chirality operator is [11,34]

$$\chi_n = \vec{\sigma}_n \cdot (\vec{\sigma}_{n+1} \times \vec{\sigma}_{n+2}), \quad (2)$$

where $\vec{\sigma}_n = (\sigma_n^x, \sigma_n^y, \sigma_n^z)$ is the spin vector of Pauli operators and the u, v couplings are real numbers with dimensions of energy. This model is a modified XX model with an additional three-spin interaction term χ, as shown in Fig. 1(a). Here we adopt periodic boundary conditions with $\vec{\sigma}_N = \vec{\sigma}_0$. If we introducing $\sigma_n^{\pm} = (\sigma_n^x \pm i\sigma_n^y)/2$, then by employing the Jordan-Wigner transformation defined by $\sigma_n^+ = (-1)^{\Sigma_n} c_n$ where $\Sigma_n = \sum_{m<n} c_m^\dagger c_m$ and $\sigma^z = 2c_n^\dagger c_n - 1$ [35], we can

map the Hamiltonian to

$$\begin{aligned} H = \sum_{n=0}^{N-1} \Bigg\{ &- u c_n^\dagger c_{n+1} - \frac{iv}{2} c_n^\dagger c_{n+2} \\ &- \frac{iv}{2} [c_n^\dagger c_{n+1}(2c_{n+2}^\dagger c_{n+2} - 1) \\ &- c_{n+1}^\dagger c_{n+2}(2c_n^\dagger c_n - 1)] \Bigg\} + \text{H.c.}, \end{aligned} \quad (3)$$

where c_n are a set of fermionic modes obeying the anti-commutation relations $\{c_n, c_m\} = \{c_n^\dagger, c_m^\dagger\} = 0$ and $\{c_n, c_m^\dagger\} = \delta_{mn}$. We see that the model is intrinsically interacting as the fermionic Hamiltonian contains quartic terms.

To analyze the behavior of the interacting model, we apply mean-field theory (MFT) to transform the Hamiltonian into an effective quadratic Hamiltonian which can be efficiently diagonalized. MFT defines the fluctuation of an operator A as $\delta A = A - \langle A \rangle$, where $\langle A \rangle$ is the expectation value of the operator A with respect to the mean-field ground state $|\Omega\rangle$. For a product of two operators we have

$$AB = \langle A \rangle B + A \langle B \rangle - \langle A \rangle \langle B \rangle + \delta A \delta B, \quad (4)$$

where the second order in fluctuations can be ignored. Applying this to the interacting terms of Eq. (3), the Hamiltonian becomes

$$\begin{aligned} H_{\text{MF}}(\alpha, Z) = \sum_{n=0}^{N-1} &\left[-(u - ivZ)c_n^\dagger c_{n+1} - \frac{iv}{2} c_n^\dagger c_{n+2} \right] \\ &+ \mu \sum_{n=0}^{N-1} c_n^\dagger c_n + E_0 + \text{H.c.}, \end{aligned} \quad (5)$$

where $\mu = 2v\,\text{Im}(\alpha)$ is an effective chemical potential controlling the number of particles in the ground state, $E_0 = v(Z-1)\text{Im}(\alpha)$ is a constant energy shift, and $\langle \sigma_n^z \rangle = Z$, $\langle c_n^\dagger c_{n+1} \rangle = \alpha$, where the expectation value is done with respect to the ground state of the mean-field Hamiltonian, $|\Omega(\alpha, Z)\rangle$, for given values of α and Z. Self-consistency requires $\langle \Omega(\alpha, Z)|\sigma_n^z|\Omega(\alpha, Z)\rangle = Z$ and $\langle \Omega(\alpha, Z)|c_n^\dagger c_{n+1}|\Omega(\alpha, Z)\rangle = \alpha$ for all n. While these two equations have many solutions, we can single one out on physical grounds: The original Hamiltonian of Eq. (3) has particle-hole symmetry, $[H, U] = 0$, where U is the particle-hole transformation with $U c_n U^\dagger = (-1)^n c_n^\dagger$ and $U c_n^\dagger U^\dagger = (-1)^n c_n$. This symmetry implies that $\langle c_n^\dagger c_n \rangle = 1/2$ and $\langle c_n^\dagger c_{n+1} \rangle \in \mathbb{R}$ in the ground state. If we require the MFT to retain the particle-hole symmetry, then these conditions imply that $Z = \mu = \alpha = 0$, and the MFT Hamiltonian becomes

$$H_{\text{MF}} = \sum_{n=0}^{N-1} \left(-u c_n^\dagger c_{n+1} - \frac{iv}{2} c_n^\dagger c_{n+2} \right) + \text{H.c.} \quad (6)$$

Another way to show the vanishing of α is that particle-hole symmetry implies that α must be real. However, in Eq. (5) we see that α only appears via $\text{Im}(\alpha)$, which is zero if particle-hole symmetry is applied and therefore vanishes from H fully.

This Hamiltonian is quadratic and periodic, hence it can be diagonalized with a Fourier transform,

$$c_n = \frac{1}{\sqrt{N}} \sum_{p \in \text{B.Z.}} e^{ianp} c_p, \quad (7)$$

where B.Z. $= [-\pi/a, \pi/a)$ is the Brillouin zone, p are the momenta quantized as $p = 2n\pi/Na$ for $n \in \mathbb{Z}$, c_p are the momentum space fermionic modes, and a is the lattice spacing. This brings the Hamiltonian into the diagonal form

$$H_{\text{MF}} = \sum_{p \in \text{B.Z.}} E(p) c_p^\dagger c_p, \quad (8)$$

where the dispersion relation is given by

$$E(p) = -2u \cos(ap) + v \sin(2ap), \quad (9)$$

as shown in Fig. 1. The Fermi points of this model, defined as the points $\{p_i\}$ such that $E(p_i) = 0$, are given by $p_\pm = \pm \pi/2a$ for $|v| < |u|$, while for $|v| \geqslant |u|$ we find two additional Fermi points located at

$$p_1 = \frac{1}{a} \sin^{-1} \left(\frac{u}{v} \right), \quad p_2 = \frac{\pi}{a} - p_1, \quad (10)$$

as shown in Fig. 1(b). These additional points arise due to the Nielsen-Ninomiya theorem.

B. Phase transitions

To investigate the nature of quantum phases supported by Eq. (1), and the transitions between them, we consider the case of homogeneous couplings u and v along the chain. In this section, we focus on the predictions of the mean-field Hamiltonian of Eq. (6) and compare it with the results obtained using matrix product state analysis of the spin Hamiltonian of Eq. (1) [9]. All analytic calculations of this section are done using the mean-field theory.

1. Correlations

The correlation matrix is defined as $C_{nm} = \langle \Omega | c_n^\dagger c_m | \Omega \rangle$, where $|\Omega\rangle$ is the ground state of Hamiltonian (6). Mapping to momentum space with a discrete Fourier transform as in Eq. (7), we can write

$$C_{nm} = \frac{1}{N} \sum_{p,q \in \text{B.Z.}} e^{-ipn} e^{iqm} \langle \Omega | c_p^\dagger c_q | \Omega \rangle$$

$$= \frac{1}{2\pi} \sum_{p:E(p)<0} \Delta p \, e^{-ip(n-m)}$$

$$= \frac{1}{2\pi} \int_{p:E(p)<0} dp \, e^{-ip(n-m)}, \quad (11)$$

where in the second equality we used the fact that the ground state $|\Omega\rangle$ has all negative energy states occupied, so $\langle \Omega | c_p^\dagger c_q | \Omega \rangle = \delta_{pq} \theta[-E(p)]$ and used the fact that eigenstates are separated in momentum space by $\Delta p = 2\pi/N$ for a lattice spacing $a = 1$ to rewrite the sum as a Riemann sum. In the third equality we took the thermodynamic limit $N \to \infty$ mapping the sum to an integral which can now be solved analytically.

For $|v| < |u|$ the correlation function is given by

$$C_{nm} = \frac{\sin \left[\frac{\pi}{2}(n-m) \right]}{\pi(n-m)}. \quad (12)$$

For $|v| > |u|$, the negative energy portion of the Brillouin zone splits into two disconnected regions so the integral splits into two as

$$C_{nm} = \frac{1}{2\pi} \left(\int_{-\frac{\pi}{2}}^{p_1} dp + \int_{\frac{\pi}{2}}^{\pi - p_1} dp \right) e^{-ipa(n-m)}$$

$$= \frac{i}{2\pi(n-m)} \left\{ -2 \cos \left[(n-m)\frac{\pi}{2} \right] + (-1)^{n-m} e^{ip_1(n-m)} + e^{-ip_1(n-m)} \right\}, \quad (13)$$

which is now a function of v and is not smooth. The fact the correlation matrix is not a smooth function of v is a consequence of the change in topology of the Fermi sea shown by the gray portion of Fig. 1. As observables are derived from the correlation matrix, this behavior is the root cause of the phase transition exhibited by the model.

2. Energy density

The ground state $|\Omega\rangle$ is the state for which the Fermi sea is fully occupied. Therefore, the ground-state energy density is given by

$$\rho_0 = \frac{1}{N} \langle \Omega | H | \Omega \rangle \to \frac{1}{2\pi} \int_{p:E(p)<0} dp \, E(p), \quad (14)$$

where we took the thermodynamic limit $N \to \infty$ by using the standard trick of moulding the sum into a Riemann sum and taking the limit. We have

$$\rho_0 = \begin{cases} -\frac{2u}{\pi} & |v| \leqslant |u| \\ -\frac{1}{\pi} \left(\frac{u^2}{v} + v \right) & |v| > |u|. \end{cases} \quad (15)$$

If we look at the derivatives of the energy density, then we see that the model exhibits a second-order phase transition as we change v. The first derivative of ρ_0 is continuous, but there exists a discontinuity in the second derivative as

$$\frac{\partial^2 \rho_0}{\partial v^2} = \begin{cases} 0 & |v| \leqslant |u| \\ -\frac{1}{\pi} \frac{u^2}{v^3} & |v| > |u| \end{cases}, \quad (16)$$

revealing that the point $|v| = |u|$ corresponds to the critical point of a second-order phase transition.

In Fig. 2, we compare the ground-state energy density vs v for the MPS numerics of the spin model [9] and the mean-field approximation for a system of $N = 200$. We see that the mean field agrees well with the spin model, accurately predicting the location of the critical point. Below the critical point, the two models agree exactly, which suggests that the interactions induced by the chiral term are irrelevant in the ground state. Nevertheless, interactions become significant above the critical point.

3. Central charge

To gain further insight into the nature of the chiral phase transition, we consider the behavior of the ground-state bipartite entanglement entropy as a function of v. Consider
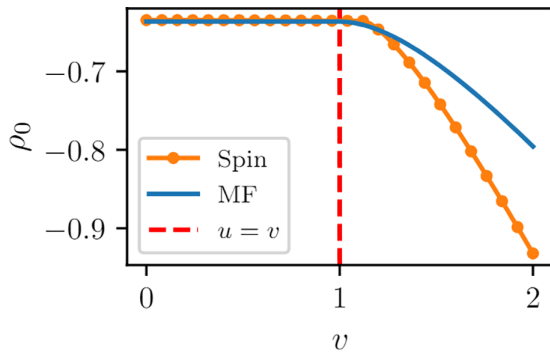
FIG. 2. A comparison of the ground-state energy density vs v obtained from MPS simulation of the spin model from Ref. [9] and the mean-field (MF) approximation for $N = 200$ spins.

partitioning the system into two subsystems, $\mathcal{A}$ and $\mathcal{B}$, where $\mathcal{A}$ contains $L \ll N$ adjacent spins. We define the reduced density matrix of $\mathcal{A}$ as the partial trace over the remaining $N - L$ spins of $\mathcal{B}$ as $\rho_{\mathcal{A}} = \mathrm{Tr}_{\mathcal{B}}(\rho)$, where ρ is the state of the whole system. As we are interested in the ground state only, we have $\rho = |\Omega\rangle\langle\Omega|$, where $|\Omega\rangle$ is the (pure) ground state of the total system. The entanglement entropy is defined as $S_{\mathcal{A}} = -\mathrm{Tr}(\rho_{\mathcal{A}} \ln \rho_{\mathcal{A}})$. As discussed above, the model is gapless for all v so it can be described by a conformal field theory (CFT) [36]. In this case we expect the ground-state entanglement entropy of a partition of spins to obey the Cardy formula,

$$S_{\mathcal{A}}^{\mathrm{PBC}}(L) = \frac{c}{3} \ln L + S_0, \tag{17}$$

provided $L \ll N$, and where c is the central charge of the CFT and S_0 is a constant [10,37], which applies to both the original spin model and the mean-field approximation but differ for open (OBC) and periodic (PBC) and boundary conditions. We can measure the entanglement entropy of the mean-field model (for PBC) quite simply by using the correlation matrix. We find that scaling behavior of the entanglement entropy follows the formula in Eq. (17), as shown in Fig. 3(a), allowing us to extract the central charge c for various values of v. We
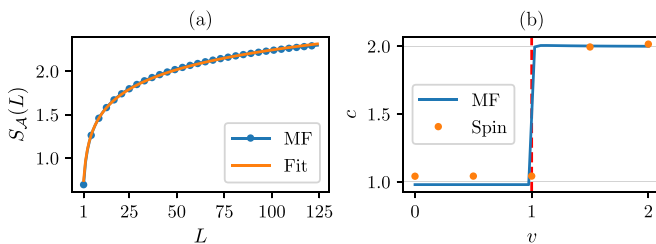

FIG. 3. (a) The entanglement entropy S_L of the mean-field (MF) model vs L for a system of size $N = 500$, for values $u = 1$ and $v = 0.5$ with periodic boundary conditions. We see the entanglement entropy follows Eq. (17), allowing us to extract the central charge. (b) A comparison of the central charge c of the mean-field model and spin model vs v for the same system. We see that the central charge jumps from $c = 1$ to $c = 2$ across the phase transition for the mean field, suggesting that the degrees of freedom of the model have changed. The central charge for the spin model was calculated using OBC and fitted using Eq. (2) in Ref. [10].

find good agreement with the Cardy formula at even small L, we expect this is due to the primary operators that define the CFT being localized on single lattice sites, similarly to the *XY* model. Therefore no RG flow is necessary to access the universal behavior.

Using the MPS results with open boundary conditions we compare the spin model and the mean-field approximation. In Fig. 3(b) we see that $c \approx 1$ in the XX phase which jumps to $c \approx 2$ in the chiral phase, with good agreement between the spin and mean-field results. We can clearly interpret this in the mean-field model: The additional Fermi points appearing when $|v| > |u|$ cause the model to transition from a $c = 1$ CFT with a single Dirac fermion to a $c = 2 = 1 + 1$ CFT with two Dirac fermions, as seen by the additional Fermi points of the dispersion in Fig. 1(b). This can also be understood from the lattice structure of the MF model, as seen in Fig. 1(a), where for $|v| \ll |u|$ a single zigzag fermionic chain dominates ($c = 1$) while for $|v| \gg |u|$ two fermionic chains dominate, corresponding to the edges of the ladder, thus effectively doubling the degrees of freedom ($c = 2$).

III. EMERGENT BLACK HOLE BACKGROUND

A. Diatomic model

To make the link with relativity, the lattice sites are now labeled as alternating between sublattices A and B by introducing a two-site unit cell, as shown in Fig. 4. The mean-field Hamiltonian of Eq. (6) can be reparameterized as

$$H_{\mathrm{MF}} = \sum_n -u a_n^{\dagger}(b_n + b_{n-1}) - \frac{iv}{2}(a_n^{\dagger} a_{n+1} + b_n^{\dagger} b_{n+1}) + \mathrm{H.c.}, \tag{18}$$

where the fermionic modes a_n and b_n belong to sublattice A and B, respectively, of the unit cell located at site n. These modes obey the commutation relations $\{a_n, a_m^{\dagger}\} = \{b_n, b_m^{\dagger}\} = \delta_{nm}$, while all mixed anticommutators vanish. The index n now labels the unit cells. A Fourier transform is performed on the Fermions with the definition

$$a_n = \frac{1}{\sqrt{N_c}} \sum_{p \in \mathrm{B.Z.}} e^{i p a_c n} a_p, \tag{19}$$

and similarly for b_n, where $N_c = N/2$ is the number of unit cells in the system, $a_c = 2a$ is the unit cell spacing for a given lattice spacing a, and B.Z. $= [0, 2\pi/a_c)$ is the Brillouin zone. The Fourier transformed Hamiltonian becomes

$$H_{\mathrm{MF}} = \sum_{p \in \mathrm{B.Z.}} \chi_p^{\dagger} h(p) \chi_p, \quad h(p) = \begin{bmatrix} g(p) & f(p) \\ f^*(p) & g(p) \end{bmatrix}, \tag{20}$$

where the two-component spinor is defined as $\chi_p = (a_p, b_p)^T$ and the functions are given by

$$f(p) = -u(1 + e^{-i a_c p}), \quad g(p) = v \sin(a_c p). \tag{21}$$

As usual, the dispersion relation is given by the eigenvalues of the single-particle Hamiltonian $h(p)$ which yields

$$E(p) = g(p) \pm |f(p)|$$
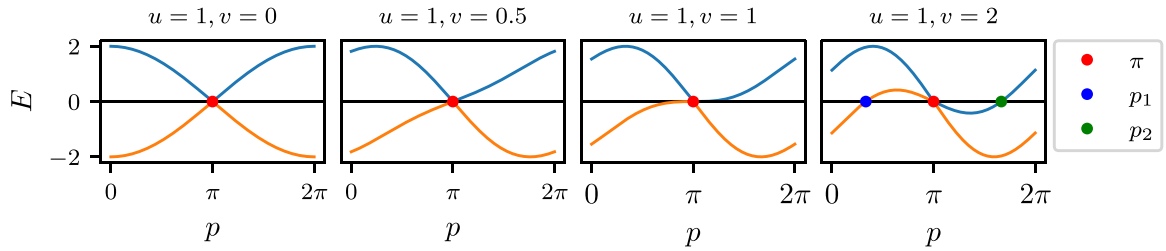$$= v \sin(a_c p) \pm u \sqrt{2 + 2\cos(a_c p)}. \tag{22}$$

FIG. 4. The tilting of the Dirac cones as v increases and $u = 1$. The blue and orange sections show the dispersions of the two operators a and b, respectively, in the diatomic unit cell for $a_c = 1$.

Clearly, this energy spectrum is not the same as the one we derive from Eq. (1); however, we are only interested in the ground-state properties, which are seen throughout this paper, such as in Fig. 7, to agree exactly for $v < u$, and diverge slightly for $v > u$.

In Fig. 4, it is found that the parameter v has the effect of tilting the cones as it increases. The Fermi points $\{p_i\}$, defined as the points for which $E(p_i) = 0$, are found at

$$p_0 = \frac{\pi}{a_c}, \quad p_\pm = \pm\frac{1}{a_c}\arccos\left(1 - \frac{2u^2}{v^2}\right). \quad (23)$$

The roots $p_\pm$ only exist if the argument of arccos is in the range $[-1, 1]$ which implies $|v| \geqslant |u|$ for these to appear in the dispersion. Therefore, if $|v| \leqslant |u|$, then the only Fermi point is located at $p_0 = \pi/a_c$ which is where the Dirac cone is located, as shown in Fig. 4. When the cone overtilts, so when $|v| \geqslant |u|$, then the additional zero-energy crossings at $p_\pm$ appear which is due to the Nielsen-Ninomiya theorem which states that the number of left- and right-movers must be equal [38].

B. Continuum limit

The continuum limit is obtained by Taylor expanding the single-particle Hamiltonian $h(p)$ about the Fermi point p_0 to first order in momentum which yields

$$h(p_0 + p) = u\sigma^y p - v\mathbb{I}p \equiv e_a{}^i\alpha^a p_i, \quad (24)$$

where we have set $a_c = 1$; the coefficients are defined as $e_0{}^x = -v$, $e_1{}^x = u$; and the Dirac matrices $\alpha^0 = \mathbb{I}$, $\alpha^1 = \sigma^y$. Therefore, the continuum limit Hamiltonian after an inverse Fourier transform to real space is given by

$$H = \int_\mathbb{R} dx\, \chi^\dagger(x)(-ie_a{}^i\alpha^a\overset{\leftrightarrow}{\partial}_i)\chi(x), \quad (25)$$

with $A\overset{\leftrightarrow}{\partial}_\mu B = \frac{1}{2}[A\partial_\mu B - (\partial_\mu A)B]$ and the Dirac $\alpha^a = (\mathbb{I}, \sigma^y)$ and $\beta = \sigma^z$. Note that the position is now measured in terms of unit cells with two lattice sites rather than single sites.

Comparing this Hamiltonian to the general one of Dirac particles in curved space [39], the continuum limit of the lattice model can be interpreted as a curved space field theory with zweibein

$$e_a{}^\mu = \begin{pmatrix} 1 & -v \\ 0 & u \end{pmatrix}, \quad e^a{}_\mu = \begin{pmatrix} 1 & v/u \\ 0 & 1/u \end{pmatrix} \quad (26)$$

and Dirac gamma matrices $\gamma^0 = \sigma^z$ and $\gamma^1 = -i\sigma^x$ which obey the anticommutation relations $\{\gamma^a, \gamma^b\} = 2\eta^{ab}$, with

$\eta^{ab} = \mathrm{diag}(1, -1)$. The zweibein corresponds to the metric $g_{\mu\nu} = e^a{}_\mu e^b{}_\nu \eta_{ab}$ which gives

$$ds^2 = \left(1 - \frac{v^2}{u^2}\right)dt^2 - \frac{2v}{u^2}dt\,dx - \frac{1}{u^2}dx^2. \quad (27)$$

If the variables u and v are upgraded to slowly varying functions of space, then the preceding calculation is still valid and the event horizon is located at the point x_h, where $|v(x_h)| = |u(x_h)|$. In the small region in which v is a slowly varying functions of x so the coupling of different momentum modes will be small and can be ignored to a good approximation, leaving the diagonal terms $a_p^\dagger a_p$ only. This is quite standard to do, for example, in the SSH model where the continuum is described by a Dirac equation [16]. For coordinate-dependent coefficients, this is the Gullstrand-Painlevé metric [40], also know as the *acoustic metric*, which is the Schwarzschild metric of a $(1 + 1)$D black hole expressed in Gullstrand-Painlevé coordinates. This metric is referred to here as an *internal metric* of the model as it depends on the internal couplings of the Hamiltonian and not the physical geometry of the lattice. In addition, this is a fixed classical background metric and the quantum fields have no back-reaction on the metric.

In order to bring the metric Eq. (27) into standard form, a coordinate transformation defined as $(t, x) \mapsto (\tau, x)$ is used, where

$$\tau(t, x) = t - \int_{x_0}^x dz\, \frac{v(z)}{u^2 - v^2(z)}, \quad (28)$$

that maps the metric to

$$ds^2 = \left[1 - \frac{v^2(x)}{u^2(x)}\right]d\tau^2 - \frac{1}{u^2(x)\left[1 - \frac{v^2(x)}{u^2(x)}\right]}dx^2, \quad (29)$$

which takes the general form of the Schwarzschild metric. As we are interested in the physics of the horizon we consider only the behavior of the the system for $x \approx x_h$ where $f(x)$ can be taken to have a linear profile that changes sign around $x = x_h$ and satisfies $f(x_h) = 0$, this condition corresponding to $v(x_h) = u$ in the couplings of our model. In the following we take $u(x) = 1$ so it aligns with the standard Schwarzschild metric in natural units. Quite remarkably, if we look at the condensed matter model with space-dependent parameters $u(x)$ and $v(x)$, then the phase boundary between the regions for $|v| < u$ and $|v| > u$, as seen in Fig. 8, can be interpreted in terms of a field theory with a black-hole metric, where the phase boundaries align precisely with the event horizons of this metric.
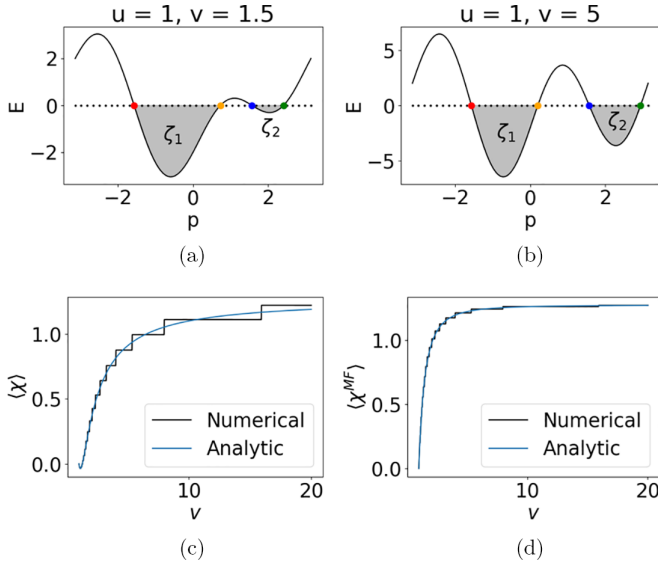
FIG. 5. The dispersion relations, with colored Fermi-points corresponding to those in Fig. 1(b), when (a) $v = 1.5$ and (b) $v = 5$, showing the difference in number of discrete momentum states (equally space momentum from $-\pi$ to π), in the spaces ζ_1 and ζ_2. (c) The chirality of any single site in a 100 site homogeneous ("flat space") lattice as v changes for the fully interacting chiral operator, with (d) giving the same for the mean-field chiral operator. Panels (c) and (d) also give the analytical solutions as given in Eqs. (38) and (39), respectively.

IV. CHIRALITY OF THE MODEL

In this section we investigate the spin-chirality operator from Eq. (2) in detail. From the previous section, we see that the parameter v has the effect of tilting the Dirac cones in the mean-field description, as shown in Fig. 4. Referring back to the original Hamiltonian of Eq. (1), we conclude that the chirality of the system is responsible for this tilting. This tilting emulates the overtilting of a Dirac cone near a black hole, and therefore it is of interest to study this operator and find what it can show about the the black-hole system, especially in the case of the spins inside of the black-hole horizon, corresponding to the transition into a chiral phase in a homogeneous lattice.

Applying the Jordan-Wigner transformation to the chirality operator of Eq. (2), we arrive at the chirality operator in terms of fermionic modes given by

$$\chi_n = -2i(c_n^\dagger c_{n+1} + c_{n+1}^\dagger c_{n+2} - c_n^\dagger c_{n+2}) \\ + 4i(c_n^\dagger c_{n+1}^\dagger c_{n+2} c_{n+2} + c_{n+1}^\dagger c_{n+2} c_n^\dagger c_n) + \text{H.c.} \quad (30)$$

It can be seen in Fig. 5(c) that the expectation of the chirality operator has a point after the transition $|v| > |u|$ where it is equal to 0. If this operator is to be viewed as an order parameter, giving the transition at the point where χ is nonzero, then it is unusual for it to return to this value. However, there is a choice now to be made of exactly which chiral operator to analyze. As the original spin Hamiltonian of Eq. (1) contains the chirality operator itself, applying MFT yields a noninteracting version of the chiral operator if we were to interpret this as the coefficient of $v/4$ in the mean-field Hamiltonian of

Eq. (6). The MFT version of the chiral operator in fermionic form is therefore given by

$$\chi_n^{\text{MF}} = 2ic_n^\dagger c_{n+2} + \text{H.c.}, \quad (31)$$

with ground-state expectation given in Fig. 5(d). In the following we will consider both versions of the chirality operator as they give complementary information. We refer to Eq. (30) as the full chirality and Eq. (31) as the mean-field chirality.

A. Discrete stepping of the chirality

In Fig. 5 it is shown how the chirality of a homogeneous chain system (corresponding to flat space) changes as the next-to-nearest neighbor terms in the Hamiltonian becomes more dominant. Clear discrete jumps in the value of chirality are found as the parameter v is increased, corresponding to a momentum state leaving the left-hand Fermi sea (denoted as ζ_1) as a momentum state enters the right-hand Fermi sea (denoted as ζ_2). This is due to the fact that the number of discrete momentum states in the total Fermi sea is equal to $N/2$, i.e., $|\zeta_1| + |\zeta_2| = N/2$, where $|\zeta_i|$ is the number of momentum states in ζ_i. As v changes, these two disconnected regions of the Fermi sea change size and hence exchange states to keep the total fixed at $N/2$.

We can determine analytically the behavior of the chirality jumps shown in Fig. 7. The total chirality in this instance can be diagonalized by the Fourier transform that also diagonalizes the Hamiltonian of the system,

$$c_n = \frac{1}{\sqrt{N}} \sum_{p \in \text{B.Z.}} e^{ipan} c_p, \quad (32)$$

to give

$$\langle \chi \rangle = -4 \sum_{p \in \text{B.Z.}} \sin(2ap) \\ - \frac{8}{N} \sum_{p,k \in \text{B.Z.}} \{\sin[a(k - 2p)] + \sin[a(p - 2k)]\}, \quad (33)$$

where the summed momenta p and k satisfy $E(p) \leqslant 0$ and $E(k) \leqslant 0$. The chirality is seen to jump in discrete steps as the chiral coupling v is increased. This diagonalized total chirality can be used to find an analytical formula for the size of the jumps. We have

$$\lim_{\epsilon \to 0} \langle \chi(v + \epsilon) \rangle - \langle \chi(v) \rangle \\ = \sqrt{1 - \frac{u^2}{v^2}} \left\{ \frac{16u}{v} - \frac{32}{N} \sum_{p \in \text{B.Z.}} \left[\sin(2p) - \frac{2u}{v} \cos(p) \right] \right\}. \quad (34)$$

In the large-v limit where the chiral operator becomes dominant we have

$$\lim_{v \to \infty} \Delta \langle \chi \rangle = -\frac{32}{N} \sum_p \sin(2p), \quad (35)$$

which gives a value of about 10.2 for the limit the jumps tend towards as v is increased. Additionally, we find that when N becomes significantly large, then

$$\lim_{N \to \infty} \Delta \langle \chi \rangle = \sqrt{1 - \frac{u^2}{v^2}} \left[\frac{16u}{v} + \frac{32}{\pi} \left(1 + \frac{u^2}{v^2} \right) \right]. \quad (36)$$
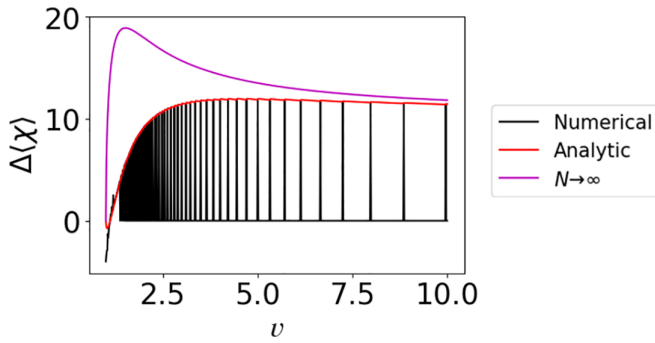
FIG. 6. Measurements of the discrete jumping of total chirality as chiral coefficient v is increased. The numerical solutions are found by taking the expectation of the chirality operator on the ground state at v and then subtracting that from the same operator for some small change $v + \epsilon$. The analytic solution is found from Eq. (33) and the thermodynamic solution $N \rightarrow \infty$ from Eq. (36).

Note that the order of the limits allows us to take $N \rightarrow \infty$ without forming a continuum version of the lattice model, as we already assumed the existence of the discrete stepping feature in Eq. (34). This analytically predicted behavior of chirality jumps is in agreement with the numerical findings, as shown in Fig. 6.

The frequency of the jumps is controlled by the rate in which the momentum space covered by ζ_1 shrinks while ζ_2 grows, as shown in Fig. 5. This can be expressed in terms of the proportion of the momentum space in the Brillouin zone that is spanned by $\zeta_1 = [\frac{-\pi}{2a}, p_1)$ for Fermi point $p_1 = \frac{1}{a} \sin^{-1}(\frac{u}{v})$. The number of states in the left-hand Fermi sea is given by

$$N_1 = N \cdot \frac{p_1 + \frac{\pi}{2a}}{2\pi} = \frac{N \sin^{-1}(u/v) + N\pi/2}{2\pi a}, \quad (37)$$

which, in Fig. 7, shows a correspondence between N_1 dropping by an integer amount to the number of discrete steps in chirality taken.

B. Chirality in the thermodynamic limit

In this section we analyze the chirality in the thermodynamic limit for $N \rightarrow \infty$. Using the expression for the correlation matrix derived in Eqs. (12) and (13), the ground-
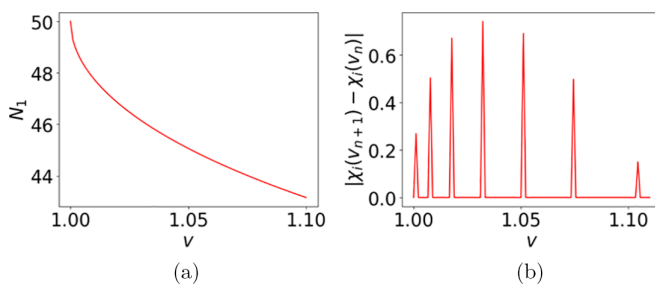

FIG. 7. (a) The jumping rate of the chirality as found from Eq. (37) and (b) the discrete jumping found from applying Eq. (33). It is seen that as the number of states in ζ_1 decreases, each integer change corresponds to a sudden increase in the chirality, with seven total jumps in this interval.
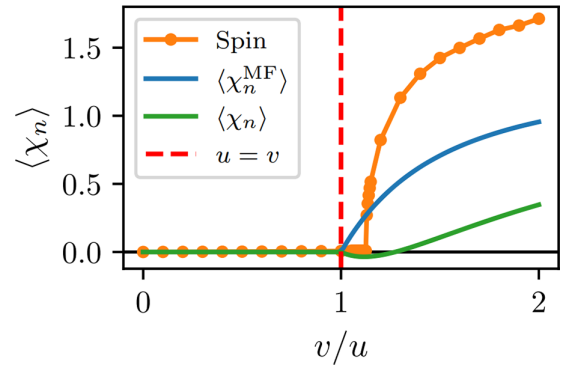

FIG. 8. A comparison of the ground-state chirality obtained from the mean-field ground state $|\Omega\rangle$ using the two operators χ and χ^{MF} [operators distinguished in Eq. (30) and Eq. (31) respectively], and the results obtained from exact diagonalization of the spin model.

state chirality with respect to the full chiral operator of Eq. (30) is given by the simple expression

$$\langle \chi_n \rangle = 8\mathrm{Im}[C_{n,n+1}C_{n+2,n+2} - C_{n,n+2}C_{n+2,n+1}$$
$$+ C_{n+1,n+2}C_{n,n} - C_{n+1,n}C_{n,n+2}$$
$$- (C_{n,n+1} + C_{n+1,n+2} - C_{n,n+2})/2]$$
$$= \begin{cases} 0 & |v| < |u| \\ \frac{4}{\pi}\left(1 - \frac{u^2}{v^2}\right)\left(\frac{4u}{\pi v} - 1\right) & |v| \geqslant |u| \end{cases}, \quad (38)$$

and for the mean-field chirality

$$\langle \chi_n^{\mathrm{MF}} \rangle = 4\mathrm{Im}(C_{n,n+2}) = \begin{cases} 0 & |v| < |u| \\ \frac{4}{\pi}\left(1 - \frac{u^2}{v^2}\right) & |v| \geqslant |u| \end{cases}. \quad (39)$$

By Taylor expanding just above the critical point, we find the chirality goes as

$$\langle \chi_n \rangle \sim (v - v_{\mathrm{c}})^\gamma, \quad (40)$$

where $v_{\mathrm{c}} = u$ is the critical point and $\gamma = 1$ is the critical exponent. On the other hand, it was shown in Ref. [9] by studying the full spin model of Eq. (1) using finite DMRG [41] that the phase transition of the full model is located at $v_{\mathrm{c}} \approx 1.12u$ with a critical exponent of $\gamma \approx 0.39$. A comparison between the chirality of this MPS spin model simulation and the mean-field approximation can be seen in Fig. 8. The mean-field faithfully captures the important information about the phase transition. In particular, just like for the energy density, the two models agree exactly below the critical point where the chirality is zero. The behavior suggests the chirality is an order parameter for the model and emphasizes again that, below the critical point, the interactions are irrelevant in the ground state. We see that the free fermion mean-field approximation of Eq. (6) accurately reveals that for small v the system is in a disordered, gapless, XX phase, while as v increases it passes through a second-order phase transition into a gapless chiral phase, corresponding to a nonzero ground-state chirality $\langle \chi_n \rangle$.

From Eqs. (38) and (39), we see that the chirality is nonzero if and only if we have complex next-to-nearest-neighbor correlations $C_{n,n+2}$. We ask under what conditions is this the case. Consider a general tight-binding model with

discrete translational symmetry and periodic boundary conditions. Suppose we had a model with inversion symmetry under the transformation $n \to -n$. This implies that the dispersion relation is an even function obeying $E(p) = E(-p)$, so our Fermi points come in $\pm$ pairs. Referring back to the definition of the correlation matrix in Eq. (11), we see that $C_{nm}^* = C_{nm}$ for an even dispersion relation: Complex conjugation is equivalent to the transformation $p \to -p$ in the integral and, as the range of integral is symmetric under this transformation due to the Fermi points being $\pm$ symmetric as the dispersion relation is an even function, the integral, and hence correlation matrix, is invariant and hence real. In fact, this condition for inversion symmetry can be relaxed slightly: As long as the Fermi points come in $\pm$ pairs, even if the dispersion $E(p)$ itself is not an even function, the correlation matrix is real. This is the case for this model in the range $|v| \leqslant |u|$ as in this phase the Fermi points are fixed at $p_0 = \pm\pi/2a$ despite the dispersion itself not being even, as shown in Fig. 1. However, this is broken when $|v| > |u|$ as new Fermi points appear and the correlation matrix is complex.

Let us now break inversion symmetry. A simple model that breaks inversion symmetry is a model with nearest-neighbor hoppings and complex couplings, with Hamiltonian

$$H = -ue^{-i\theta} \sum_n c_n^\dagger c_{n+1} + \text{H.c.}, \tag{41}$$

where $u \in \mathbb{R}$ and $\theta \in [0, 2\pi)$. The breaking of inversion symmetry is apparent from the dispersion relation $E(p) = -2u\cos(p - \theta)$ as it is no longer an even function. The Fermi points of this model are at $p_0 = \theta \pm \pi/2$, and therefore the correlations of this model are given by

$$
\begin{aligned}
C_{nm} &= \frac{1}{2\pi} \int_{\theta-\frac{\pi}{2}}^{\theta+\frac{\pi}{2}} dp\, e^{-ip(n-m)} \\
&= \frac{\sin\left[(n-m)\frac{\pi}{2}\right]}{\pi(n-m)} e^{-i\theta(n-m)},
\end{aligned} \tag{42}
$$

which are complex, but notice that correlations between next-to-nearest-neighbors, where $|n - m| = 2$, are zero, and therefore the chirality of this model will be zero, too.

The simplest way to achieve complex next-to-nearest neighbor correlations is to include a term in the Hamiltonian which couples next-to-nearest neighbor sites and breaks inversion symmetry. A simple example of this is nothing but our mean-field Hamiltonian of Eq. (6). The interesting feature of this model is that for $|v| < |u|$, the dispersion relation retains its symmetric Fermi points at $p_\pm = \pm\pi/2$ despite the dispersion not being symmetric. Therefore, all correlators in this phase will be real as seen in Eq. (12) and hence the chirality will be zero. On the other hand, for $|v| > |u|$ the dispersion relation changes resulting in complex correlations which yields a nonzero chirality, giving the chirality its order parameter behavior.

C. Black-hole profile chiralities

The above analysis was conducted for homogeneous systems where u and v are constants. However, we still expect this to hold when we upgrade v to a slowly varying function. We now consider profiles where $v(x)$ changes slowly and
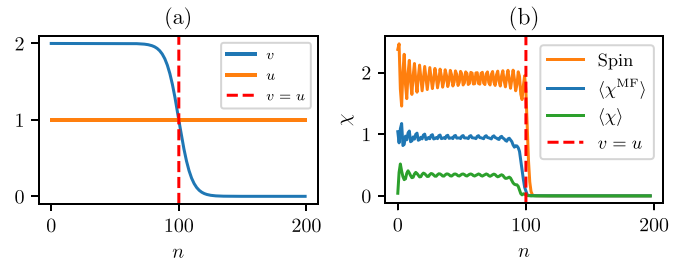

FIG. 9. (a) An example of an inhomogeneous distribution for the couplings v. (b) The corresponding chirality obtained from the spin model MPS [9] and the mean-field model with the full operator χ. We see that the distribution of v describes a phase boundary between a chiral ($v > u$) and nonchiral ($v < u$) phase.

investigate the behavior of the system around $v = u$, which from the emergent metric in Eq. (27), corresponds to the location of the event horizon. In Fig. 9 we present the chirality distribution across the system for a given coupling profile $v(x)$ for constant u. We observe the result that the system is chiral where $|v| > |u|$, whereas for $|v| < |u|$ the system is nonchiral, and therefore we have an interface between two phases.

The chirality expectation can be found for different blackhole backgrounds by choosing an appropriate relation for v. If a collapsing dust metric for a black hole is considered, then the coupling becomes

$$v = \sqrt{1 - M(|x| - x_h/2)}, \tag{43}$$

where M is the mass of the black hole and x_h is the position of its horizon [42]. Another useful metric is a hyperbolic tanh profile [43], with coupling

$$v = \alpha\{\tanh[\beta(x - x_h) + \delta] + 1\}, \quad \delta = \tanh^{-1}\left(\frac{1}{\alpha} - 1\right). \tag{44}$$

In Fig. 10 we present the chiralities across the lattice, where the position on the lattice x corresponds to the position in space. Moreover, we present the total chiralities of these black-hole profiles as their parameters are altered, giving similar results to those in the homogeneous case.

It has been shown that many analog gravitational systems will exhibit a Hawking-like effect, whereby emission of radiation is described by scattering events following a thermal distribution at the Hawking temperature [15–26,28–30]. This has been explicitly demonstrated in the mean-field model of Eq. (6) with inhomogenous couplings, whereby interfaces between the two chiral phases thermalizes the wave function [9]. By preparing a single particle inside the horizon in the state $|n\rangle = c_n^\dagger|0\rangle$ and letting it evolve under the Hamiltonioan, it is found that once the wave-function tunnels across the horizon the external distribution takes the form $P(k, t) \propto e^{-E(k)/T}$, where T is the Hawking temperature of the effective black hole given by $T = |v'(x_h)|/2\pi$. This is an effective thermalization exhibited shortly after the scattering [14,15].

V. BOSONIZATION

We now want to quantify the effect of interactions in our system introduced via the chirality term and analyze the
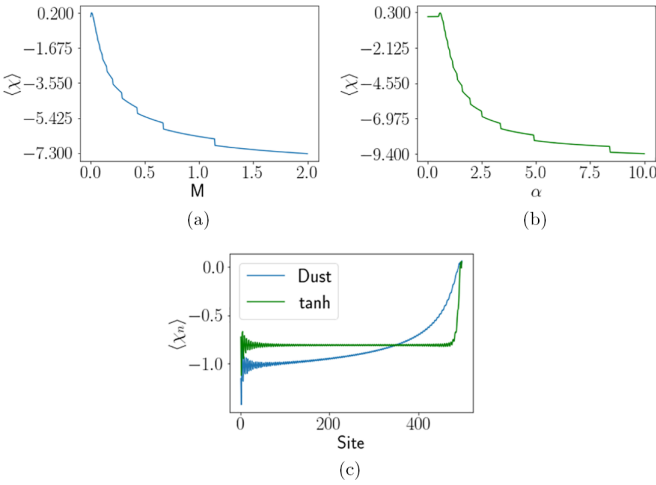
FIG. 10. [(a) and (b)] Measurements of total chirality for 100 sites lattices with the horizon x_h at site 95 for the collapsing dust profile when mass M is increased and then for the hyperbolic tanh profile as α is increased respectively. (c) Chirality expectations of each site of a 500 site lattice for spatial functions $v(x)$ with horizon x_h positioned at site 450 for the collapsing dust metric with $M = 1$ (blue) and with the hyperbolic profile of v couplings as in Eq. (44) with $\alpha = 2$, $\beta = 0.2$ (green).

validity of the mean-field results. In higher dimensions, most interacting fermionic models can be studied using Fermi liquid theory. One dimensional systems can differ dramatically. The breakdown of Fermi liquid theory is intuitively explained by the nature of excitations near the Fermi surface [32]. In one dimension, the Fermi surface consists of two points, k_F and $-k_F$. For inversion-symmetric Hamiltonians, the dispersion in the vicinity of the Fermi surface is typically $\omega_1(k) = v_F(k - k_F)$ and $\omega_2(k) = -v_F(k - k_F)$. The *nesting condition* $\omega_1(k) = -\omega_2(k)$ leads to a breakdown in perturbation theory and indicates that the interacting model differs dramatically from the noninteracting model. In fact, the low-energy behavior is typically described by collective, bosonic excitations using Luttinger liquid theory.

For the model discussed here, bosonization has been previously employed when $|v| < |u|$ in which case there are only two Fermi points [9]. This resulted in the bosonized Luttinger liquid Hamiltonian

$$H = u \int dx [\Pi^2 + (\partial_x \Phi)^2] \tag{45}$$

for a bosonic field Φ with canonical momentum Π. This corresponds to a Luttinger coefficient [32] $K = 1$, corresponding to a free fermion model in the whole regime with the interactions simply renormalizing the Fermi velocities. This can be simply understood by noting that the Fermi velocities differ at the two Fermi points, and therefore the nesting condition does not apply.

When $|v| > |u|$ there are two additional Fermi points with equal Fermi velocites so the nesting condition becomes relevant. The bosonized system is now described by a four-component Hamiltonian given, neglecting terms with minimal

contribution, by

$$H = \sum_{\mu,\nu} \partial_x \phi_\mu h_{\mu\nu} \partial_x \phi_\nu \tag{46}$$

where ϕ_μ represents the bosonic fields [31] centered at each Fermi point in the sum of μ and ν and

$$h_{\mu\nu} = \frac{1}{\pi} \begin{pmatrix} \frac{\pi v_{L_1}}{2} - 2v & 0 & v - u & v - u \\ 0 & \frac{\pi v_{L_2}}{2} + 2v & u - v & u - v \\ v - u & u - v & \frac{\pi v_R}{2} + 2u & 2u \\ v - u & u - v & 2u & \frac{\pi v_R}{2} + 2u \end{pmatrix}, \tag{47}$$

with Fermi velocities $v_{L_{1,2}} = 2(\mp u - v)$ and $v_R = 2v(1 - \frac{u^2}{v^2})$. After a coordinate transformation we find, near the transition point $v \approx u$, the Hamiltonian takes the form

$$H = u \int dx [\Pi_1^2 + (\partial_x \Phi_1)^2]$$
$$+ \sqrt{v_R v_R'} \int dx \left[\sqrt{\frac{v_R}{v_R'}} \Pi_2^2 + \sqrt{\frac{v_R'}{v_R}} (\partial_x \Phi_2)^2 \right], \tag{48}$$

for bosonic fields Φ_1, Φ_2 and corresponding canonical momenta Π_1, Π_2, giving Luttinger coefficients of $K_1 = 1$ and $K_2 = \sqrt{v_R/v_R'} = \sqrt{v_R/(v_R + \frac{8u}{\pi})}$. Since the Luttinger coefficient $K_2 \neq 1$, the interactions after the transition into the chiral phase are relevant and have a significant influence on the model.

VI. CLASSICAL ANALYSIS

To gain further insight into the behavior of the chiral spin chain we analyze the classical version of the model. Classically, the spins are unit vectors that can take arbitrary orientations. The dispersion is found by minimizing the energy of the spin vectors in a classically equivalent energy function. The Hamiltonian is now given as

$$H = \sum_n \left[-\frac{u}{2} \left(S_n^x S_{n+1}^x + S_n^y S_{n+1}^y \right) - \frac{v}{4} \vec{S}_n \cdot (\vec{S}_{n+1} \times \vec{S}_{n+2}) \right], \tag{49}$$

for spin $\vec{S}_n = (\sin \phi_n \cos \theta_n, \sin \phi_n \sin \theta_n, \cos \phi_n)$. We adopt open boundary conditions, so the summation in Eq. (49) ends at $N - 2$ for the chiral operator. The u controlled XX portion of the energy tends to align all the spins with nearest-neighbor couplings while the chiral coupling v of the three-spin interaction, tends to make neighboring spins orthogonal. The overall spin configuration that minimizes the energy was determined numerically, where the first site was set as spin up and all others sites were free, and the classical chirality found using DMRG.

The average chirality has the form

$$\langle \chi \rangle = \frac{1}{N} \sum_n \vec{S}_n \cdot (\vec{S}_{n+1} \times \vec{S}_{n+2}). \tag{50}$$

The value for chirality for the spin configurations that minimize the classical energy is given in Fig. 11. By showing the spins along the chain in Bloch space it can be seen that, when
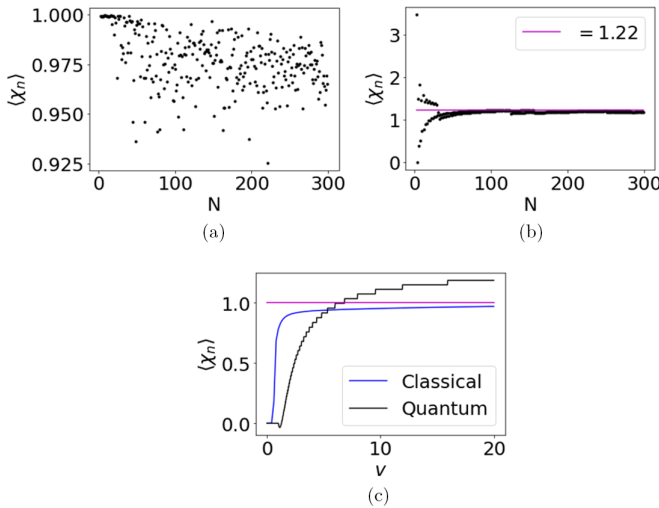
FIG. 11. (a) Average chirality, when $u = 1$, $v = 20$, with the strong chiral contribution from large v gives almost 1 as lattice size N is increased for the classical chain, compared to the quantum case in (b) for values up to $N = 300$, which shows similar, locally oscillatory behavior with a tendency toward ~1.22 as lattice size is increased. (c) Values for the classical/quantum chirality operator, given in blue/black, as v is increased for a periodic lattice of $N = 300$. The classical value slowly approaches 1, while the quantum chirality grows larger towards ~1.22. It can also be seen that the classical chirality begins to grow before the transition point of $u = v$.

$v > u$, the spin structure of the lattice is a repeating three-spin sequence with these three spins almost orthogonal due to the chiral operator minimizing while the spins are orthogonal, whereas the XX portion of the energy is minimized when the spins are parallel. This sequence then repeats along the lattice while slowly processing, as is shown in Fig. 12, where the effect of increasing the chiral coupling strength is given.

The results from Fig. 11 show a similarity between the classical chirality calculations and those done in the quantum case. This figure also gives the changes in average chirality χ when the system size is increased, shown to be a tendency toward 1 in the classical regime as the spins align for every extension of the chain to maximize the chirality. From observing the spins Fig. 12 when v is large it is found the spins take on a repeating three-spin pattern in which they attempt to stay orthogonal to maximize χ, which may increase by a maximum of 1 for every chiral operator acted along the chain.
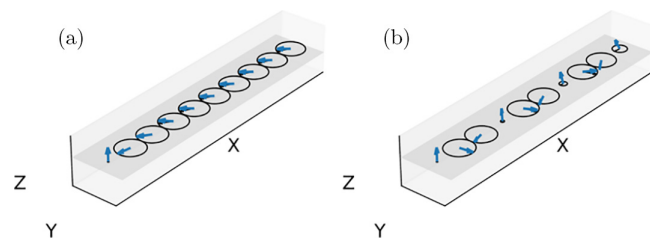

FIG. 12. The procession of spins in a 10 spin lattice as found by the classical model for (a) $v = 0.8$ and (b) $v = 8$. In (b) the spin states are found in sets of three almost orthogonal spins that repeats and processes along the chain.

In contrast, in the quantum chain the chirality takes a maximal value of approximately 1.22, as shown in Fig. 11. This indicates that chirality receives contributions from genuine quantum correlations, which causes its value to become larger than the maximum possible classical value of 1 [11].

VII. CONCLUSION

While the one-dimensional XX model supports the relativistic one-dimensional Dirac equation, adding a chiral interaction causes the Dirac code to tilt an effect that is controlled by the chiral coupling. Surprisingly, this emulates the effect of gravitational background on Dirac fermions [9]. When the chiral coupling varies appropriately as a function of position then the chiral spin chain simulates the behavior of Dirac particles in the black-hole background.

In particular, we introduced a chiral spin model and simplified it with MFT in order to investigate its properties analytically. This included the dispersion relation, which exhibited transition shown by a splitting of the Fermi sea of the half filled ground state, and the central charge, giving what kind of CFT is defined by the transition of the system into a chiral phase. Results were then compared to an MPS simulation to give an idea of the accuracy of this mean-field Hamiltonian.

Subsequently, we assessed the field theory defined by splitting the spin chain model into a diatomic unit cell and found a comparison to the field theory of Dirac particles on the curved spacetime background of a black hole with the curvature determined by the couplings of the model. It is seen, by the dispersion relation of the diatomic model, that increasing the relative strength of the chiral coupling tilts the energy spectrum, analogously to the overtilting of the Dirac cone as it enters the horizon of a black hole.

To determine the contribution of the chiral interactions in the behavior of the system we employed the bosonization method. This method determines the importance of the interactions, in turn giving an insight into the accuracy of the noninteracting approach that was taken in applying MFT to the Hamiltonian. Before the splitting of the Fermi sea, bosonization gave a Luttinger coefficient of $K = 1$, implying the interactions are insignificant. After the sea splits, i.e., for $v > u$, two separate coefficients emerge, corresponding to the two portions of the Fermi sea. One of them has a value different than 1, suggesting the interactions after the transition into the chiral phase have a significant influence on the model.

Finally, the classical version of the model is investigated. An energy function analogous to the quantum chain Hamiltonian was minimized in order assess the behavior of chirality in the classical limit. We established that for large chiral coupling the spin vectors tend to be orthogonal, with a three-spin pattern processing along the chain. Importantly, the quantum chain gives a value of chirality larger than then possible classical value, thus demonstrating that quantum correlations contribute significantly in the behavior of the system.

We envision that our work can build the bridge between chiral systems and black holes, thus facilitating the quantum simulation of Hawking radiation, e.g., with cold atom technology. Moreover, our investigation opens the way for modeling certain strongly correlated systems by effective geometric

theories with extreme curvature, thus providing an intuitive tool for their analytical investigation. As the bosonization of the system in the chiral phase appears to indicate the interactions are important in this regime, a comparison between this model and that of a solveable quantum gravity could be a future focus of research, e.g., via measuring the scrambling of our model.

APPENDIX A: ON THE SPACE-TIMELIKENESS OF THE BLACK HOLE

In the Gullstrand-Painlevé frame, the metric is given by

$$ds^2 = (1 - v^2)dt^2 - 2vdtdx - dx^2, \quad (A1)$$

where we have set $u = 1$. Consider the vectors $T^\mu = \delta_t^\mu$ and $X^\mu = \delta_x^\mu$ which point in the t and x directions, respectively. We have

$$g_{\mu\nu}T^\mu T^\nu = g_{tt} = (1 - v^2), \quad (A2)$$

$$g_{\mu\nu}X^\mu X^\nu = g_{xx} = -1, \quad (A3)$$

so we see that the time coordinate is spacelike inside the black hole ($v > 1$) and timelike outside ($v < 1$) the black hole as the norm of T^μ changes sign. However, the x coordinate remains spacelike everywhere as the norm of X^μ is negative everywhere. This is fine because, despite this, the metric is still Lorentzian everywhere. This means at every point there exists a spacelike and timelike direction, they just do not coincide with the coordinates in the GP frame. To see this we just need to solve for the eigenvalues of the metric, which are given by

$$\mu_\pm = \tfrac{1}{2}(\pm\sqrt{v^4 + 4} - v^2), \quad (A4)$$

where $\mu_+ > 0$ and $\mu_- < 0$ always. Therefore, the metric is Lorentzian and there will exist a pair of spacelike and timelike directions at every point. This contrasts to a Euclidean metric which would have only positive eigenvalues.

If we change coordinates from GP coordinates to the Schwarzschild frame as $(t, x) \to (\tau, \chi)$ where

$$\tau(t, x) = t - \int_{x_0}^x dz \frac{v(z)}{1 - v^2(z)}, \quad (A5)$$

$$\chi(t, x) = x, \quad (A6)$$

where we have explicitly used a different symbol for the spatial coordinate χ despite it being equal to x always, then we have

$$ds^2 = (1 - v^2)d\tau^2 - \frac{1}{(1 - v^2)}d\chi^2. \quad (A7)$$

If apply the same procedure as before, then we have

$$g_{\tau\tau} = 1 - v^2, \quad (A8)$$

$$g_{\chi\chi} = -\frac{1}{1 - v^2}, \quad (A9)$$

which always have opposite signs, and therefore if τ is timelike, then χ is spacelike and vice versa. We see that in this coordinate system, the coordinate basis vectors do point along the spacelike and timelike directions explicitly. Note that despite the transformation $\chi(t, x) = x$ being trivial, the basis vectors for x and χ do not point in the same direction.

APPENDIX B: DIAGONALIZING THE CHIRALITY OPERATOR

The ground-state expectation of the total chirality operator, given simply by the sum of the chirality for every site in the lattice, may be diagonalized by applying a the Fourier transform given in Eq. (7). Utilizing Wick's theorem [9], the expectation of the chirality takes the form

$$
\begin{aligned}
\langle \chi_i \rangle = &-2i(\langle c_n^\dagger c_{n+1} \rangle + \langle c_{n+1}^\dagger c_{n+2} \rangle + \langle c_{n+2}^\dagger c_n \rangle) \\
&+ 4i(\langle c_n^\dagger c_{n+1} \rangle \langle c_{n+2}^\dagger c_{n+2} \rangle - \langle c_n^\dagger c_{n+2} \rangle \langle c_{n+2}^\dagger c_{n+1} \rangle \\
&+ \langle c_{n+1}^\dagger c_{n+2} \rangle \langle c_n^\dagger c_n \rangle - \langle c_{n+1}^\dagger c_n \rangle \langle c_n^\dagger c_{n+2} \rangle) + \text{c.c.},
\end{aligned}
$$
$$(B1)$$

where $\langle c_i^\dagger c_j \rangle = \langle \Omega | c_i^\dagger c_j | \Omega \rangle$ where $|\Omega\rangle$ is the ground state of the system corresponding to half filling. The transform has the effect

$$
\begin{aligned}
\sum_n \langle \chi_n \rangle = &\sum_{p,q} -2i(e^{iaq} + e^{-ia(p-2q)} + e^{-2iap})\left(\frac{1}{N}\sum_n e^{-ian(p-q)}\right)\langle c_p^\dagger c_q \rangle \\
&+ \sum_{p,q,k,l} \frac{4i}{N}(e^{-ia(2k-q-2l)} - e^{-ia(2k-2q-l)} + e^{-ia(p-2q)} - e^{-ia(p-2l)})\left(\frac{1}{N}\sum_n e^{-ian(p-q+k-l)}\right)\langle c_p^\dagger c_q \rangle \langle c_k^\dagger c_l \rangle + \text{c.c.} \\
= &\sum_p -2i(2e^{iap} + e^{-2iap})\langle c_p^\dagger c_p \rangle + \sum_{q,k,l} \frac{4i}{N}\left\{2e^{iaq} - e^{-ia(k-2q)} - e^{-ia(q-2k)})\langle c_{q+l-k}^\dagger c_q \rangle \langle c_k^\dagger c_l \rangle + \text{c.c.} \right. \\
= &\sum_p [8\sin(ap) - 4\sin(2ap)]\langle c_p^\dagger c_p \rangle + \frac{4i}{N}\sum_{p,k}[2e^{iap} - (e^{-ia(k-2p)} + e^{-ia(p-2k)}] + \text{c.c.} \left.\right\}\langle c_p^\dagger c_p \rangle \langle c_k^\dagger c_k \rangle, \quad (B2)
\end{aligned}
$$

which, considering the half filling ground state, simplifies to

$$
\sum_n \chi_n = \sum_p [8\sin(ap) - 4\sin(2ap)] - \sum_p 8\sin(ap)
$$
$$
- \frac{8}{N}\sum_{p,k}\{\sin[a(k-2p)] + \sin[a(p-2k)]\}
$$
$$
= -4\sum_p[\sin(2ap)]
$$
$$
- \frac{8}{N}\sum_{p,k}\{\sin[a(k-2p)] + \sin[a(p-2k)]\}, \quad (B3)
$$

for the summations only accounting for momenta which produce negative energy solutions. Here the fact that the ground-state expectations follow the rule

$$
\langle c_p^\dagger c_q \rangle = \begin{cases} \delta_{pq} & \text{if } E(p) \geqslant 0 \text{ and } E(q) \geqslant 0 \\ 0 & \text{if } E(p) < 0 \text{ or } E(q) < 0 \end{cases}, \quad (B4)
$$

meaning $\sum_p \langle c_p^\dagger c_p \rangle = \frac{N}{2}$ was utilized.

In order to find an analytical solution for the size and frequency of these jumps the fact the jumps originate from the "hopping" of momentum states from the space ζ_1 to the space ζ_2 is utilized. If the chirality is known to change in a discrete step at certain points the parameter v increasing by an infinitesimilly small amount δv, then the amplitude in the difference in the total chirality is therefore given by $\chi(v_\delta) - \chi(v)$. From the Fermi points found in the dispersion relation Fig. (1) it is seen the momentum states that contributing to chirality differences as v increases are those momenta lost at $v = \sin^{-1}(\frac{u}{v})$ and those gained at $v_\delta = \pi - \sin^{-1}(\frac{u}{v})$. This gives

$$
\chi(v_\delta) - \chi(v) = 4\left[\sum_{p_v}\sin(2ap_v) - \sum_{p_{v_\delta}}\sin(2ap_{v_\delta})\right]
$$
$$
+ \frac{8}{N}\sum_{p_v,k_v}[\sin(k_v - 2p_v) + \sin(p_v - 2k_v)]
$$
$$
- \frac{8}{N}\sum_{p_{v_\delta},k_{v_\delta}}[\sin(k_{v_{\text{new}}} - 2p_{v_\delta}) + \sin(p_{v_\delta} - 2k_{v_\delta})]. \quad (B5)
$$

Substituting in the identities for the momentum states gives

$$
\lim_{v_\delta \to v}\chi(v_\delta) - \chi(v)
$$
$$
= \frac{16u}{v}\sqrt{1 - \frac{u^2}{v^2}} - \frac{32}{N}\sum_p\left[\sqrt{1 - \frac{u^2}{v^2}}\sin(2p)\right.
$$
$$
\left. - \frac{2u}{v}\sqrt{1 - \frac{u^2}{v^2}}\cos(p)\right], \quad (B6)
$$

which may be used to estimate the size of the jumps, as used in Fig. 1.

Different limits show that value of the jumps at different extremes. When the chiral term dominates $v \to \infty$, giving

$$
\lim_{v\to\infty}\lim_{v_\delta\to v}\langle\chi(v_\delta)\rangle - \langle\chi(v)\rangle = \frac{-32}{N}\sum_p\sin(2p), \quad (B7)
$$

which gives a value of about 10.2. In the thermodynamic limit $N \to \infty$ where $\frac{1}{N}\sum_p \to \frac{1}{\pi}\int_p$ the change in chirality becomes

$$
\lim_{N\to\infty}\lim_{v_+\to v}\langle\chi(v_+)\rangle - \langle\chi(v)\rangle
$$
$$
= \frac{16u}{v}\sqrt{1 - \frac{u^2}{v^2}} + \frac{32}{\pi}\sqrt{1 - \frac{u^2}{v^2}}\left(1 + \frac{u^2}{v^2}\right), \quad (B8)
$$

which is shown in Fig. 6.

APPENDIX C: TWO FERMI-POINT BOSONIZATION

1. Normal ordering

The Hamiltonian may be separated into noninteracting and interacting systems $H = H_0 + H_{\text{int}}$ for

$$
H_0 = \sum_n\left(-uc_n^\dagger c_{n+1} - \frac{iv}{2}c_n^\dagger c_{n+2}\right) + \text{H.c.}, \quad (C1)
$$

$$
H_{\text{int}} = \frac{iv}{2}\sum_n\left(c_n^\dagger c_{n+1}\sigma_{n+2}^z + c_{n+1}^\dagger c_{n+2}\sigma_n^z\right) + \text{H.c.} \quad (C2)
$$

Normal ordering, $:A: = A - \langle\Omega|A|\Omega\rangle$, affects Fermionic operators as

$$
c_n^\dagger c_{n+1} = :c_n^\dagger c_{n+1}: +\langle\Omega|c_n^\dagger c_{n+1}|\Omega\rangle \equiv :c_n^\dagger c_{n+1}: +\alpha, \quad (C3)
$$

and

$$
\sigma_n^z = 1 - 2c_n^\dagger c_n = 1 - 2(:c_n^\dagger c_n: +\langle\Omega|c_n^\dagger c_n|\Omega\rangle)
$$
$$
= -2:c_n^\dagger c_n:, \quad (C4)
$$

where the fact the ground state is a state of half filling gives $\langle\Omega|c_n^\dagger c_n|\Omega\rangle = \frac{1}{2}$. Therefore, the interacting Hamiltonian becomes

$$
H_{\text{int}} = -iv\sum_n(:c_n^\dagger c_{n+1}: +\alpha):c_{n+2}^\dagger c_{n+2}:
$$
$$
+ (:c_{n+1}^\dagger c_{n+2}: +\alpha):c_n^\dagger c_n: +\text{H.c.}
$$
$$
= -iv\sum_n :c_n^\dagger c_{n+1}::c_{n+2}^\dagger c_{n+2}:
$$
$$
+ :c_{n+1}^\dagger c_{n+2}::c_n^\dagger c_n: +\text{H.c.}, \quad (C5)
$$

where the fact that α is real and $:c_n^\dagger c_n:$ is Hermitian cancels α out of the calculation.

It has been found that in the nonchiral phase where $|v| < |u|$ there are two Fermi points at momenta $\pm\pi/2$.

2. Field transformations

A real space continuum is approximated with field relations

$$
\frac{c_n}{\sqrt{a}} = \sum_{\mu=R,L}e^{ip_\mu an}\psi_\mu(x_n), \quad (C6)
$$

where the sum is over the Fermi points and $\psi_\mu(x_n)$ is a slowly varying continuous field sampled at discrete lattice sites $x_n = na$, with reinstated lattice spacing a.

First, we substitute the expansion of Eq. (C6) into H_0 of Eq. (C2) to give

$$H_0 = \sum_{\mu,\nu} \sum_n a e^{-i(p_\mu - p_\nu)an} - u e^{ip_\nu a} \psi_\mu^\dagger(x_n) \psi_\nu(x_{n+1})$$
$$- \frac{iv}{2} e^{2ip_\nu a} \psi_\mu^\dagger(x_n) \psi_\nu(x_{n+2}) + \text{H.c.} \quad \text{(C7)}$$

We now discard any oscillating term in the Hamiltonian as these integrate to zero, so we requires $p_\mu = p_\nu$ in the first phase. This yields

$$H_0 = \sum_\mu \sum_n a(-u e^{ip_\mu a} \psi_\mu^\dagger \psi_\mu + a\partial_x \psi_\mu)$$
$$- \frac{iv}{2} e^{2ip_\mu a} \psi_\mu^\dagger (\psi_\mu + 2a\partial_x \psi_\mu) + O(a^3) + \text{H.c.}$$
$$= -i \sum_\mu \sum_n a^2 (\pm u \psi_\mu^\dagger \partial_x \psi_\mu - v \psi_\mu^\dagger \partial_x \psi_\mu) + O(a^3) + \text{H.c.}$$
$$\to -2i \sum_\mu \int dx\, v_\mu \psi_\mu^\dagger \partial_x \psi_\mu, \quad \text{(C8)}$$

where in the third line $\pm$ corresponds to $\mu = R, L$ for the right- and left-hand Fermi points, and we have renormalized the couplings as $au \to u$ and $av \to v$. We have defined

$$v_{R,L} = 2(\pm u - v), \quad \text{(C9)}$$

which are the Fermi velocities $v_\mu = E'(p_\mu)$ obtained from the dispersion relation.

We now repeat the procedure for the interaction term H_{int} of Eq. (C2). We substitute in the expansion of Eq. (C6) into H_{int} to give

$$H_{\text{int}} = -iv \sum_{\mu,\nu,\alpha,\beta} \sum_n a e^{-i(p_\mu - p_\nu + p_\alpha - p_\beta)an}$$
$$\times (e^{i[p_\nu - 2(p_\alpha - p_\beta)]a} + e^{-i(p_\mu - 2p_\nu)a}) : \psi_\mu^\dagger \psi_\nu :: \psi_\alpha^\dagger \psi_\beta :$$
$$+ O(a^3) + \text{H.c.}, \quad \text{(C10)}$$

where we have expanded all fields to zeroth order in a to ensure the Hamiltonian retains order a^2 and renormalized the couplings as $av \to v$. We discard any term that oscillates which requires $p_\mu - p_\nu + p_\alpha - p_\beta = 2n\pi/a$ for $n \in \mathbb{Z}$. With this we find only four terms survive giving us

$$H_{\text{int}} = 2v \int dx (\rho_R^2 + \rho_R \rho_L - \rho_L \rho_R - \rho_L^2) + \text{H.c.}$$
$$= 4v \int dx (\rho_R^2 - \rho_L^2), \quad \text{(C11)}$$

where we have defined the normal-ordered densities $\rho_{R,L} := \, : \psi_{R,L}^\dagger \psi_{R,L} :.$

3. Bosonizing the Hamiltonian

If we pull everything together, then the normal-ordered Hamiltonian is given by

$$: H : \, = \, : H_0 + H_{\text{int}} :$$
$$= -i \sum_{\mu=R,L} \int dx \big(v_\mu : \psi_\mu^\dagger \partial_x \psi_\mu : \pm 4v : \rho_\mu^2 :\big), \quad \text{(C12)}$$

where the $\pm$ corresponds to R and L, respectively. Following Ref. [31], we map the fermionic fields ψ_μ to bosonic fields ϕ_μ with the mapping

$$\psi_{R,L} = F_{R,L} \frac{1}{\sqrt{2\pi\alpha}} e^{-i\sqrt{2\pi}\phi_{R,L}}$$
$$\rho_{R,L} = \mp \frac{1}{\sqrt{2\pi}} \partial_x \phi_{R,L}, \quad \text{(C13)}$$

where $F_{R,L}$ are a pair of Klein factors and α is a cutoff. The bosonic fields obey the commutation relations

$$[\phi_{R,L}(x), \phi_{R,L}(y)] = \pm \frac{i}{2} \text{sgn}(x - y), \quad \text{(C14)}$$

while pairs of fields about different Fermi points commute. The fermionic fields and densities obey the identities

$$: \psi_{R,L}^\dagger \partial_x \psi_{R,L} := \pm \frac{i}{2} \partial_x \phi_{R,L}, \quad \rho_{R,L} = \mp \frac{1}{\sqrt{2\pi}} \partial_x \phi_{R,L}, \quad \text{(C15)}$$

where we have taken lattice length $L \to \infty$. With this, the Hamiltonian is mapped to

$$: H : \, = \int dx \frac{1}{2} [|v_R| : (\partial_x \phi_R)^2 : + |v_L| : (\partial_x \phi_L)^2 :]$$
$$+ \frac{2v}{\pi} [(\partial_x \phi_R)^2 - (\partial_x \phi_L)^2]$$
$$= \frac{1}{2} \int dx [|v_R'| : (\partial_x \phi_R)^2 : + |v_L'| : (\partial_x \phi_L)^2 :], \quad \text{(C16)}$$

where the renormalized Fermi velocities are given by

$$v_{R,L}' = 2\left[\pm u - v\left(1 - \frac{2}{\pi}\right)\right]. \quad \text{(C17)}$$

As the Fermi velocities of the model are not equal, we must generalize the bosonization procedure of Ref. [31]. We define the canonical transformation

$$\Phi = \sqrt{\frac{\mathcal{N}}{2}} (\sqrt{|v_L'|}\phi_L - \sqrt{|v_R'|}\phi_R)$$
$$\Theta = \sqrt{\frac{\mathcal{N}}{2}} (\sqrt{|v_L'|}\phi_L + \sqrt{|v_R'|}\phi_R), \quad \text{(C18)}$$

where $\mathcal{N}$ is a constant to ensure the fields obey the correct commutation relations. We require the fields Φ and Θ to obey the commutation relations [31]

$$[\Phi(x), \Theta(y)] = -\frac{i}{2} \text{sgn}(x - y). \quad \text{(C19)}$$

In terms of our canonical transformation, we have

$$
\begin{aligned}
[\Phi(x), \Theta(y)] &= \frac{\mathcal{N}}{2}(|v_L'|[\phi_L(x), \phi_L(y)] - |v_R'|[\phi_R(x), \phi_R(y)]) \\
&= \frac{\mathcal{N}}{2}\left[-\frac{i|v_L'|}{2}\mathrm{sgn}(x-y) - \frac{i|v_R'|}{2}\mathrm{sgn}(x-y)\right] \\
&= -\frac{i\mathcal{N}}{4}(|v_L'| + |v_R'|)\mathrm{sgn}(x-y),
\end{aligned}
\tag{C20}
$$

and therefore we require

$$
\mathcal{N} = \frac{2}{|v_L'| + |v_R'|} = \frac{1}{2u}.
\tag{C21}
$$

Inverting the canonical transformation of Eq. (C18), we have

$$
\sqrt{|v_L'|}\phi_- = \sqrt{u}(\Theta + \Phi), \quad \sqrt{|v_R'|}\phi_+ = \sqrt{u}(\Theta - \Phi).
\tag{C22}
$$

Substituting this back into the bosonized Hamiltonian of Eq. (C16) gives

$$
: H := u \int dx [: (\partial_x \Theta)^2 : + : (\partial_x \Phi)^2 :].
\tag{C23}
$$

Differentiating the commutator $[\Phi(x), \Theta(y)]$ with respect to y, we find $[\Phi(x), \partial_y \Theta(y)] = i\delta(x-y)$, so we can identify the canonical momentum as $\Pi(x) = \partial_x \Theta(x)$. Therefore, the bosonized Hamiltonian takes the form of the free boson,

$$
: H := u \int dx [: \Pi^2 : + : (\partial_x \Phi)^2 :],
\tag{C24}
$$

which is exactly the same result obtained from bosonizing the XX model ($v = 0$). According to the theory of Luttinger liquids, this implies that $K = 1$ which is the sign of noninteracting fermions [32], demonstrating that the interactions for $|v| < |u|$ are irrelevant in the ground state.

APPENDIX D: FOUR FERMI-POINT BOSONIZATION

1. Bosonizing for four Fermi points

When $|v| > |u|$ the chirality kicks in and two extra points are formed, shown in Fig. (1). The Fermi points will here be labeled by where they appear on the two momentum spaces $\zeta_{1,2}$, giving $p_{L_1,R_1} = \mp\pi/2$, $p_{L_2} = \sin^{-1}(u/v)$, $p_{R_2} = \pi - \sin^{-1}(u/v)$.

Just as before, the expansion of Eq. (C6) is substituted into H_0 of Eq. (C2) and oscillatory terms are disregarded, this time, for the four Fermi points. This again results in

$$
H_0 = -i \sum_\mu \int dx v_\mu \psi_\mu^\dagger \partial_x \psi_\mu,
\tag{D1}
$$

where the couplings have been renormalized as $au \to u$ and $av \to v$. New couplings are defined as

$$
v_{L_2,L_1} = 2(\pm u - v), \quad v_{R_1,R_2} = 2v\left(1 - \frac{u^2}{v^2}\right),
\tag{D2}
$$

representing the four Fermi points where $v_{L_1}, v_{R_1} \in \zeta_1$ and $v_{L_2}, v_{R_2} \in \zeta_2$ with the L and R representing the Fermi points on the left and right sides of the ζ spaces.

Repeating the procedure for the interaction term H_{int}, the new Fermi points are substituted into Eq. (C10). For the case of four Fermi points a more complicated contribution of

$$
\begin{aligned}
H_{\mathrm{int}} = av \sum_n \int dx[&-4(\rho_{L_1}\rho_{R_1} + \rho_{L_1}\rho_{R_2} + \rho_{L_2}\rho_{R_1} + \rho_{L_2}\rho_{R_2}) + 2\mathrm{Re}(d)(\psi_{R_1}^\dagger \psi_{R_2} \psi_{R_2}^\dagger \psi_{R_1} + \psi_{R_2}^\dagger \psi_{R_1} \psi_{R_1}^\dagger \psi_{R_2}) \\
&+ 2\mathrm{Re}(a)(2\psi_{L_1}^\dagger \psi_{R_1} \psi_{L_1}^\dagger \psi_{R_2} + \psi_{L_1}^\dagger \psi_{R_1} \psi_{R_1}^\dagger \psi_{L_1} + \psi_{L_1}^\dagger \psi_{R_2} \psi_{R_2}^\dagger \psi_{L_1} + \psi_{R_1}^\dagger \psi_{L_1} \psi_{L_1}^\dagger \psi_{R_1} + 2\psi_{R_1}^\dagger \psi_{L_1} \psi_{R_2}^\dagger \psi_{L_1} + \psi_{R_2}^\dagger \psi_{L_1} \psi_{L_1}^\dagger \psi_{R_2}) \\
&+ 2\mathrm{Re}(c)(\psi_{R_1}^\dagger \psi_{L_2} \psi_{L_2}^\dagger \psi_{R_1} + 2\psi_{R_1}^\dagger \psi_{L_2} \psi_{R_2}^\dagger \psi_{L_2} + \psi_{L_2}^\dagger \psi_{R_1} \psi_{R_1}^\dagger \psi_{L_2} + 2\psi_{L_2}^\dagger \psi_{R_1} \psi_{L_2}^\dagger \psi_{R_2} + \psi_{L_2}^\dagger \psi_{R_2} \psi_{R_2}^\dagger \psi_{L_2} + \psi_{R_2}^\dagger \psi_{L_2} \psi_{L_2}^\dagger \psi_{R_2}) \\
&+ 2\mathrm{Re}(b)(\rho_{R_1}\rho_{L_1} + \rho_{R_1}\rho_{L_2} + \rho_{R_2}\rho_{L_1} + \rho_{R_2}\rho_{L_2} + 2\rho_{R_1}\rho_{R_2} + \rho_{R_1}^2 + \rho_{R_2}^2)],
\end{aligned}
\tag{D3}
$$

is obtained, with density functions as defined before, and factors given as

$$
\begin{aligned}
\mathrm{Re}(a) &= \mathrm{Re}(e^{2i\sin^{-1}(u/v)} + ie^{-i\sin^{-1}(u/v)}) \\
&= 1 + \frac{u}{v} - \frac{2u^2}{v^2},
\end{aligned}
\tag{D4}
$$

$$
\mathrm{Re}(b) = \mathrm{Re}(-2ie^{i\sin^{-1}(u/v)}) = \frac{2u}{v},
\tag{D5}
$$

$$
\begin{aligned}
\mathrm{Re}(c) &= \mathrm{Re}(ie^{-i\sin^{-1}(u/v)} - e^{2i\sin^{-1}(u/v)}) \\
&= \frac{u}{v} - 1 + \frac{2u^2}{v^2},
\end{aligned}
\tag{D6}
$$

$$
\begin{aligned}
\mathrm{Re}(d) &= \mathrm{Re}(ie^{3i\sin^{-1}(u/v)} - ie^{-3i\sin^{-1}(u/v)}) \\
&= \frac{8u^3}{v^3} - \frac{6u}{v}.
\end{aligned}
\tag{D7}
$$

2. Bosonic fields

Bosonic field equations are given as in the two Fermi point model,

$$
\psi_\mu = F_\mu \frac{1}{\sqrt{2\pi\alpha}}e^{\mp i\sqrt{2\pi}\phi_\mu}, \quad \rho_\mu = \mp\frac{1}{\sqrt{2\pi}}\partial_x \phi_\mu,
\tag{D8}
$$

where the $\mp$ results are for right movers L_2, R_1, R_2 ($-$) and left movers L_1 ($+$) [movement seen from their Fermi velocities Eq. (D2)]. This gives the relation

$$
: \psi_{R,L}^\dagger \partial_x \psi_{R,L} := \pm\frac{i}{2}\partial_x \phi_{R,L},
\tag{D9}
$$

which allows the transformation H_0 from Eq. (D1) into

$$
H_0 = \frac{1}{2}\int dx \sum_\mu |v_\mu| : (\partial_x \phi_\mu)^2 :.
\tag{D10}
$$

The interacting Hamiltonian's transformation is

$$
\begin{aligned}
H_{\text{int}} = \frac{2}{\pi} \int dx \bigg\{ & v(\partial_x\phi_{L_1}\partial_x\phi_{R_1} + \partial_x\phi_{L_1}\partial_x\phi_{R_2} - \partial_x\phi_{L_2}\partial_x\phi_{R_1} - \partial_x\phi_{L_2}\partial_x\phi_{R_2}) \\
& + \frac{v}{\pi}\left(\frac{u}{v} + 1 - \frac{2u^2}{v^2}\right)\{\cos[\sqrt{2\pi}(2\phi_{L_1} + \phi_{R_1} + \phi_{R_2})] + 1\} + \frac{v}{\pi}\left(\frac{u}{v} - 1 + \frac{2u^2}{v^2}\right)\{\cos[\sqrt{2\pi}(2\phi_{L_2} - \phi_{R_1} - \phi_{R_2})] + 1\} \\
& + u[\partial_x\phi_{R_1}\partial_x\phi_{L_2} + \partial_x\phi_{R_2}\partial_x\phi_{L_2} - \partial_x\phi_{R_1}\partial_x\phi_{L_1} - \partial_x\phi_{R_2}\partial_x\phi_{L_1} + 2\partial_x\phi_{R_1}\partial_x\phi_{R_2} + (\partial_x\phi_{R_1})^2 \\
& + (\partial_x\phi_{R_2})^2] + v[(\partial_x\phi_{L_2})^2 - (\partial_x\phi_{L_1})^2] + \frac{4u^3}{v^2\pi} - \frac{3u}{\pi} \bigg\},
\end{aligned}
\tag{D11}
$$

which, when ignoring the cosine terms, in matrix form, is given as

$$
H = \left[\frac{1}{\pi}\begin{pmatrix} -2v & 0 & v-u & v-u \\ 0 & 2v & u-v & u-v \\ v-u & u-v & 2u & 2u \\ v-u & u-v & 2u & 2u \end{pmatrix} + \frac{1}{2}\begin{pmatrix} v_{L_1} & 0 & 0 & 0 \\ 0 & v_{L_2} & 0 & 0 \\ 0 & 0 & v_{R_1} & 0 \\ 0 & 0 & 0 & v_{R_2} \end{pmatrix} \right]\begin{pmatrix} \partial_x\phi_{L_1} \\ \partial_x\phi_{L_2} \\ \partial_x\phi_{R_1} \\ \partial_x\phi_{R_2} \end{pmatrix}.
\tag{D12}
$$

3. Luttinger coefficient

It is possible to approximate to Eq. (D12) as the cosine terms, if relevant in the renormalization group sense, would open a gap in the model [31], meaning it may no longer be defined by a Luttinger liquid. However, it is seen from Fig. 3(b) that the chiral phase has a central charge $c = 2$, suggesting the model is "doubly gapless," and therefore these terms cannot be significant and may be ignored. In order to diagonalize the Hamiltonian Eq. (D12)), the coordinate transformations

$$
\Phi_1 = \sqrt{\frac{1}{4u}}(\sqrt{|v'_{L_1}|}\phi_{L_1} - \sqrt{|v'_{L_2}|}\phi_{L_2})
$$

$$
\Theta_1 = \sqrt{\frac{1}{4u}}(\sqrt{|v'_{L_1}|}\phi_{L_1} + \sqrt{|v'_{L_2}|}\phi_{L_2}),
\tag{D13}
$$

$$
\Phi_2 = \frac{1}{\sqrt{2}}(\varphi_{R_1} - \varphi_{R_2})
$$

$$
\Theta_2 = \frac{1}{\sqrt{2}}(\varphi_{R_1} + \varphi_{R_2}),
\tag{D14}
$$

are considered, which gives the Hamiltonian in the form

$$
H = \frac{1}{2}\text{diag}(u, u, v_R + 8u/\pi, v_R) + \frac{1}{2}\begin{pmatrix} 0 & M \\ M^\dagger & 0 \end{pmatrix}, \tag{D15}
$$

with $M = \frac{v-u}{\pi\sqrt{2u}}\begin{pmatrix} \sqrt{|v'_{L_1}|} - \sqrt{|v'_{L_2}|} & 0 \\ \sqrt{|v'_{L_1}|} + \sqrt{|v'_{L_2}|} & 0 \end{pmatrix}$. Therefore, close to the point of transition when $u \approx v$ this becomes

$$
\begin{aligned}
H = u \int & dx[\Pi_1^2 + (\partial_x\Phi_1)^2] \\
& + \sqrt{v_R v'_R} \int dx \left[\sqrt{\frac{v_R}{v'_R}}\Pi_2^2 + \sqrt{\frac{v'_R}{v_R}}(\partial_x\Phi_2)^2 \right]. \tag{D16}
\end{aligned}
$$

This gives a Luttinger coefficient of $K_2 = \sqrt{\frac{v_R}{v'_R}} = \sqrt{\frac{v_R}{v_R + \frac{8u}{\pi}}}$. The change in value of K_2 suggests that in the chiral phase, the model has significant interactions.

[1] P. R. Wallace, The band theory of graphite, Phys. Rev. **71**, 622 (1947).

[2] A. H. Castro Neto, F. Guinea, N. M. R. Peres, K. S. Novoselov, and A. K. Geim, The electronic properties of graphene, Rev. Mod. Phys. **81**, 109 (2009).

[3] A. Farjami, M. D. Horner, C. N. Self, Z. Papić, and J. K. Pachos, Geometric description of the Kitaev honeycomb lattice model, Phys. Rev. B **101**, 245116 (2020).

[4] A. Kitaev, Anyons in an exactly solved model and beyond, Ann. Phys. **321**, 2 (2006).

[5] N. Read and D. Green, Paired states of fermions in two dimensions with breaking of parity and time-reversal symmetries and the fractional quantum Hall effect, Phys. Rev. B **61**, 10267 (2000).

[6] O. Golan and A. Stern, Probing topological superconductors with emergent gravity, Phys. Rev. B **98**, 064503 (2018).

[7] E. Lieb, T. Schultz, and D. Mattis, Two soluble models of an antiferromagnetic chain, Ann. Phys. **16**, 407 (1961).

[8] A. D. Pasquale, G. Costantini, P. Facchi, G. Florio, S. Pascazio, and K. Yuasa, XX model on the circle, Eur. Phys. J.: Spec. Top. **160**, 127 (2008).

[9] M. D. Horner, A. Hallam, and J. K. Pachos, Chiral spin-chain interfaces exhibiting event-horizon physics, Phys. Rev. Lett. **130**, 016701 (2023).

[10] G. Vidal, J. I. Latorre, E. Rico, and A. Kitaev, Entanglement in quantum critical phenomena, Phys. Rev. Lett. **90**, 227902 (2003).

[11] D. I. Tsomokos, J. J. Garcia-Ripoll, N. R. Cooper, and J. K. Pachos, Chiral entanglement in triangular lattice models, Phys. Rev. A **77**, 012106 (2008).

[12] S. W. Hawking, Particle creation by black holes, Commun. Math. Phys. **43**, 199 (1975) [Erratum: **46**, 206 (1976)].

[13] D. N. Page, Hawking radiation and black hole thermodynamics, New J. Phys. **7**, 203 (2005).

[14] M. K. Parikh and F. Wilczek, Hawking radiation as tunneling, Phys. Rev. Lett. **85**, 5042 (2000).

[15] R.-Q. Yang, H. Liu, S. Zhu, L. Luo, and R.-G. Cai, Simulating quantum field theory in curved spacetime with quantum many-body systems, Phys. Rev. Res. **2**, 023107 (2020).

[16] D. Sabsovich, P. Wunderlich, V. Fleurov, D. I. Pikulin, R. Ilan, and T. Meng, Hawking fragmentation and Hawking attenuation in Weyl semimetals, Phys. Rev. Res. **4**, 013055 (2022).

[17] D. Maertens, N. Bultinck, and K. V. Acoleyen, Hawking radiation on thelattice as universal (floquet) quench dynamics, arXiv:2204.06583.

[18] H. Huang, K.-H. Jin, and F. Liu, Black-hole horizon in the Dirac semimetal $Zn_2In_2S_5$, Phys. Rev. B **98**, 121110(R) (2018).

[19] G. E. Volovik, Black hole and Hawking radiation by type-II Weyl fermions, JETP Lett. **104**, 645 (2016).

[20] G. E. Volovik and K. Zhang, Lifshitz transitions, type-II Dirac and Weyl fermions, event horizon and all that, J. Low Temp. Phys. **189**, 276 (2017).

[21] P. Huhtala and G. E. Volovik, Fermionic microstates within the Painlevé-Gullstrand black hole, J. Exp. Theor. Phys. **94**, 853 (2002).

[22] H. Liu, J.-T. Sun, C. Song, H. Huang, F. Liu, and S. Meng, Fermionic analogue of high temperature Hawking radiation in black phosphorus, Chin. Phys. Lett. **37**, 067101 (2020).

[23] S. Guan, Z.-M. Yu, Y. Liu, G.-B. Liu, L. Dong, Y. Lu, Y. Yao, and S. A. Yang, Artificial gravity field, astrophysical analogues, and topological phase transitions in strained topological semimetals, npj Quant. Mater. **2**, 23 (2017).

[24] A. Retzker, J. I. Cirac, M. B. Plenio, and B. Reznik, Methods for detecting acceleration radiation in a Bose-Einstein condensate, Phys. Rev. Lett. **101**, 110402 (2008).

[25] A. Roldán-Molina, A. S. Nunez, and R. A. Duine, Magnonic black holes, Phys. Rev. Lett. **118**, 061301 (2017).

[26] J. Rodriguez-Laguna, L. Tarruell, M. Lewenstein, and A. Celi, Synthetic Unruh effect in cold atoms, Phys. Rev. A **95**, 013627 (2017).

[27] L. Mertens, A. G. Moghaddam, D. Chernyavsky, C. Morice, J. van den Brink, and J. van Wezel, Thermalization by a synthetic horizon, Phys. Rev. Res. **4**, 043084 (2022).

[28] M. Stone, An analogue of Hawking radiation in the quantum Hall effect, Classic. Quant. Gravity **30**, 085003 (2013).

[29] J. Steinhauer, Observation of quantum Hawking radiation and its entanglement in an analogue black hole, Nat. Phys. **12**, 959 (2016).

[30] A. Kosior, M. Lewenstein, and A. Celi, Unruh effect for interacting particles with ultracold atoms, SciPost Phys. **5**, 061 (2018).

[31] E. Miranda, Introduction to bosonization, Braz. J. Phys. **33**, 3 (2003).

[32] T. Giamarchi, *Quantum Physics in One Dimension* (Oxford University Press, Oxford, 2003).

[33] S. Aditya and D. Sen, Bosonization study of a generalized statistics model with four fermi points, Phys. Rev. B **103**, 235162 (2021).

[34] C. D'Cruz and J. K. Pachos, Chiral phase from three-spin interactions in an optical lattice, Phys. Rev. A **72**, 043608 (2005).

[35] P. Coleman, *Introduction to Many-Body Physics* (Cambridge University Press, Cambridge, UK, 2015).

[36] P. Francesco, P. Mathieu, and D. Sénéchal, *Conformal Field Theory* (Springer, New York, 2011).

[37] P. Calabrese and J. Cardy, Entanglement entropy and quantum field theory, J. Stat. Mech. (2004) P06002.

[38] H. Nielsen and M. Ninomiya, A no-go theorem for regularizing chiral fermions, Phys. Lett. B **105**, 219 (1981).

[39] S. M. Morsink and R. B. Mann, Black hole radiation of Dirac particles in 1+1 dimensions, Classic. Quant. Gravity **8**, 2257 (1991).

[40] G. E. Volovik, *The Universe in a Helium Droplet*, 2nd ed. (Clarendon Press, London, 2003).

[41] U. Schollwöck, The density-matrix renormalization group in the age of matrix product states, Ann. Phys. **326**, 96 (2011).

[42] J. Hartle, *Gravity: An Introduction to Einstein's General Relativity* (Addison Wesley, Boston, 2003).

[43] Y.-H. Shi, R.-Q. Yang, Z. Xiang, Z.-Y. Ge, H. Li, Y.-Y. Wang, K. Huang, Y. Tian, X. Song, D. Zheng, K. Xu, R.-G. Cai, and H. Fan, On-chip black hole: Hawking radiation and curved spacetime in a superconducting quantum circuit with tunable couplers, Nat. Commun. **14**, 3263 (2023).